Journal of Molecular Graphics and Modelling 59 (2015) 136–147

Contents lists available at ScienceDirect

Journal of Molecular Graphics and Modelling

journal homepage: www.elsevier.com/locate/JMGM

Phase-transition properties of glycerol–dipalmitate lipid bilayers investigated using molecular dynamics simulation

Monika Laner, Philippe H. Hünenberger*

Laboratory of Physical Chemistry, ETH Zürich, Zürich, Switzerland

ARTICLE INFO

Article history:
Accepted 22 April 2015
Available online 5 May 2015

Keywords:
Molecular dynamics
Lipid bilayer
Diglyceride
GDP
Long-timescale motions
Phase transitions

ABSTRACT

The phase- and phase-transition properties of glycerol–dipalmitate (GDP) bilayer patches are investigated using molecular dynamics simulations. This permits to characterize the influence of introducing a second aliphatic lipid tail by comparison to previously reported simulations of glycerol-1-monopalmitate (GMP). To this purpose, a set of 67 simulations (up to 300 ns duration) of $2 \times 8 \times 8$ GDP bilayer patches are performed, considering the two GDP isomers glycerol-1,3-dipalmitate (13 GDP) and glycerol-1,2-dipalmitate (12 GDP; racemic), two hydration levels (12GDP only), and temperatures in the range 250–370 K. In agreement with experiment, the GDP simulations reveal an increase in the main transition temperature by about 25 K relative to GMP, and the occurrence of non-bilayer phases at high temperatures (inverted-cylinder or stacked phases). Structurally, the GDP system tends to evidence a tighter packing of the chains, a reduced extent of tilting, increased order parameters and a reduced fluidity. These differences are easily interpreted in terms of two key changes in molecular properties when going from GMP to GDP: (i) the reduction of the headgroup polarity and hydration (from two free hydroxyl groups to a single one); (ii) the increase in the effective tail cross-section relative to the (hydrated) headgroup cross-section, conferring to GDP a particular wedge shape. These two effects contribute to the relative instability of the liquid-crystalline phase, the stability being recovered in nature when the diglyceride headgroup is functionalized by a bulky or/and polar substituent.

1. Introduction

Lipid bilayers, the main constituent of biological membranes, are of crucial importance to all living organisms because they represent the boundaries defining the different cellular compartments as well as the barrier and first interaction site to the extracellular medium [1].

Aqueous lipid systems can present many different phases [2,3] depending on the types of the lipid molecules, on their concentrations, and on the possible presence of cosolutes, as well as on pressure and temperature. The two biologically most relevant of these phases are bilayer phases, namely the gel (GL) and the liquid crystal (LC) phases [2]. In the GL phase, the aliphatic lipid tails are arranged in nearly all-*trans* conformations and in orientations that are generally tilted with respect to the bilayer normal. In the LC phase, the aliphatic tails are disordered, presenting a mixture of *trans* and *gauche* conformations, and no preferential orientation of the chains (tilting) is observed. Compared to the GL phase, the LC phase is also laterally more expanded and transversely more compact. For a given bilayer composition and under specified environmental conditions, the temperature at which the GL↔LC transition occurs is called the main transition (or melting) temperature T_m. Understanding the influence of composition and environment on this temperature as well as on the properties of the two phases is of fundamental biological and technological importance [2,4].

Atomistic molecular dynamics (MD) simulations have greatly contributed to the characterization and understanding of the structure, thermodynamics and dynamics of lipid bilayers under various conditions [5–26]. These simulations provide information at a spatial (atomic level) and temporal (femtosecond) resolution inaccessible to experiment, concerning system sizes ($\sim$ 10 nm) and timescales ($\sim 1\,\mu$s) already relevant for the evaluation of thermodynamic properties *via* statistical mechanics and the comparison with experimental data. However, the biologically most relevant phospholipids such as dipalmitoylphosphatidylcholine (DPPC) remain relatively challenging to simulate, owing to difficulties in the force-field design [27,28] and treatment of electrostatic interactions

* Corresponding author at: Laboratory of Physical Chemistry, ETH Hönggerberg, HCI, CH-8093 Zürich, Switzerland. Tel.: +41 44 632 55 03; fax: +41 44 632 10 39.
E-mail addresses: monika.laner@igc.phys.chem.ethz.ch (M. Laner), phil@igc.phys.chem.ethz.ch (P.H. Hünenberger).

http://dx.doi.org/10.1016/j.jmgm.2015.04.012
1093-3263/

[27,29–35], and to the slow convergence of system properties with respect to both system size [22,28,36–40] and simulation timescale [36,37,40–42]. For this reason, it is also interesting to consider less complex bilayer systems such as those involving monoglyceride lipids [43–52].

In a series of previous studies by our group, atomistic MD simulations have been used to characterize the phase- and phase-transition properties of a simple saturated monoglyceride, glycerol-1-monopalmitate (GMP; Fig. 1), under various environmental conditions [20–26]. Although biologically less relevant than its DPPC cousin, this model lipid represents an extraordinary testing ground for the exploration of basic bilayer properties and the formulation of qualitative principles governing them.

The next step in complexity from GMP to biologically more relevant lipids such as DPPC is the addition of a second aliphatic tail. Remaining in the context of simple esters of glycerol with palmitic acid (no headgroup functionalization), this corresponds to the two structural isomers of glycerol–dipalmitate (GDP; Fig. 1), namely glycerol-1,3-dipalmitate (13GDP) and glycerol-1,2-dipalmitate (12GDP). Note that 12GDP is a chiral molecule whereas 13GDP is not. Besides representing the simplest model lipids with two tails, diacylglycerides are actually also biologically relevant *per se*. They are involved in the metabolism of lipids [53], modulate the activity of membrane enzymes [54], participate in the transduction of extracellular signals [55], and induce structural changes in biological membranes [54,56]. The properties of diaglycerides have been studied experimentally in the context of both pure crystals and hydrated bilayers [54]. The main transition temperatures T_m for the two GDP isomers are known, namely 72–74°C and 63–66° C for 13GDP and 12GDP, respectively, based on Refs. [56–58]. The T_m values reported in earlier studies may differ by up to 10 K from these estimates [56], but consistently present a T_m difference of about 10 K between the two isomers.

In the present study, GDP bilayer patches consisting of 2×8×8 lipid molecules, either 12GDP (racemic mixture) or 13GDP, are investigated to characterize the effect of two aliphatic chains compared to only one for GMP on the structural, dynamic and thermodynamic properties of the membrane and on its main transition temperature T_m. To this purpose, a set of 67 MD simulations of up to 300 ns duration, carried out at different temperatures in the range of 250–370 K, are reported and compared. The comparison is also performed against two MD simulations of GMP at full hydration carried out at 318 and 338 K, previously reported in Refs. [22,23].

2. Methods

2.1. Molecular dynamics simulations

All MD simulations were performed using the GROMOS MD++ program [59–61], with the 53A6$_{OXY}$ force field [62] for the GMP and GDP molecules, along with the simple point charges (SPC) water model [63]. Detailed simulation and force-field information for GMP can be found in Ref. [23] and its supplementary material, and is easily transferable to GDP. The two simulations of GMP at full hydration considered here for comparison purposes have been previously reported in Ref. [23] (simulations labeled $P_NF_{GL}318$ and $P_NF_{LC}338$ therein) and the simulation details are only provided here for the new GDP simulations.

The simulations were carried out under periodic boundary conditions based on rectangular boxes containing a hydrated GDP bilayer patch of 2×8×8 lipid molecules in the *xy*-plane, leading to a total number of 128 lipid molecules in the systems. In the case of the 12GDP isomer, both leaflets consisted of a racemic mixture of the *R* and *S* enantiomers of the molecule.

Two hydration levels were considered, which are distinguished by the letters F (full) and E (elevated), respectively. The full hydration regime for GMP was defined in previous work [20,22–24] based on the phase diagram of the GMP-water system [20,43], where the main transition temperature T_m is seen to become independent of the hydration level above 6.7 water molecules per lipid. Full hydration means that in the context of a bilayer phase, water molecules added beyond this limit present very weak interactions with the lipids, so that they do not alter anymore the bilayer properties. Since the GDP molecules have two chains, an approximate doubling of the bilayer area was expected and the number of water molecules was also doubled, resulting in n_W = 1706 water molecules. This level of hydration for GDP is also referred to here as full hydration, although in view of the lower polarity of the GDP headgroup compared to that of GMP (one-half *vs.* two hydroxyl groups per tail exposed to the solvent), it is likely to already represent an excess. Some additional simulations with an even more elevated water content were also performed, involving n_W = 2559 water molecules, *i.e.* about 20 water molecules per lipid.

Newton's equations of motion were integrated using the leap-frog scheme [64] with a timestep of 2 fs. All solute bond lengths were constrained by application of the SHAKE procedure [65] with a relative geometric tolerance of 10^{-4}. The full rigidity of the water molecules was enforced by application of the SETTLE procedure [66]. The center of mass translational motion of the computational box was removed every 0.2 ps.

The simulations were carried out in the isothermal-isobaric ensemble with a reference pressure P of 1 bar and reference temperatures T ranging from 250 to 370 K. The temperature was maintained by weakly coupling [67] the solute and solvent degrees of freedom separately to temperature baths at temperature T, using a relaxation time of 0.1 ps. The pressure was maintained by weakly coupling [67] the particle coordinates and box dimensions in the *xy*-plane and along the *z*-axis separately (semi-anisotropic pressure coupling [28]) to a pressure bath at pressure P, using a relaxation time of 0.5 ps and an isothermal compressibility of 4.575×10^{-4} (kJ mol^{-1} nm^{-3})$^{-1}$ as appropriate for biomolecular systems [68].

The non-bonded interactions were calculated using a twin-range scheme [68,69], with short- and long-range cutoff distances set to 0.8 and 1.4 nm, respectively, and an update frequency of five timesteps for the short-range pairlist and intermediate-range interactions. A reaction-field correction [70,71] was applied to account for the mean effect of electrostatic interactions beyond the long-range cutoff distance, using a relative dielectric permittivity of 61 as appropriate for the SPC water model [72]. All simulations were carried out for a duration of at most 300 ns after equilibration, and configurations were saved to file every 10 ps for subsequent analysis.

2.2. Simulated systems

A total number of 67 simulations were carried out, differing by: (*i*) the GDP isomer (13GDP *vs.* 12GDP); (*ii*) the hydration level (F *vs.* E); (*iii*) the initial configuration (GL *vs.* LC *vs.* LC1 – LC3); (*iv*) the temperature T (from 250 to 370 K in steps of 20 K); (*v*) the initial pseudo-random velocities in cases of multiple repeats from a common starting configuration. Only a subset of the possible combinations was considered. The corresponding systems and conditions are summarized in Table 1, which also includes the two previously reported GMP simulations [23] for reference.

All simulations started from the original GL or LC-like structures were carried out at seven different temperatures from 250 to 370 K in steps of 20 K. However, the simulations initiated from alternative LC-like structures LC1 – LC3 (see further below) were only performed at four temperatures between 290 and 350 K, and simulation repeats started from the original GL or LC-like structures

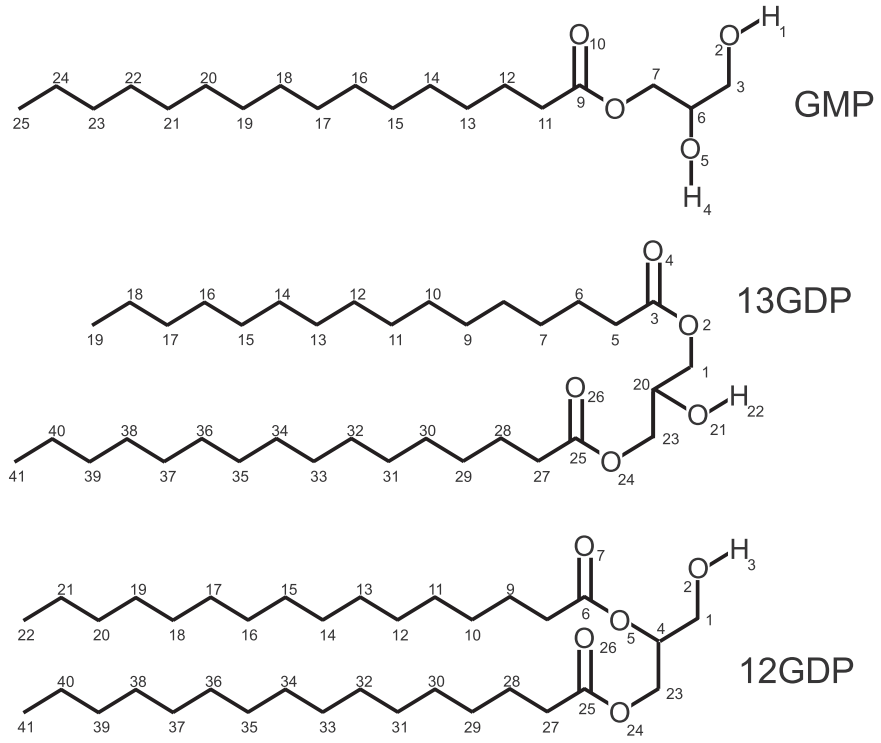

Fig. 1. Chemical structures of the mono- and diglycerides considered in the present study. The compounds are glycerol-1-monopalmitate (GMP), glycerol-1,3-dipalmitate (13GDP) and glycerol-1,2-dipalmitate (12GDP). The numbering refers to the GROMOS molecular topology used in the simulations.

Table 1
Simulated systems and simulation conditions. For each simulation, the simulation label, the hydration level (F or E for full or elevated), the number n_W of water molecules, the water concentration c_W (by weight relative to the lipids), the starting configuration (GL for gel or LC for liquid crystal; LC1 and LC2 represent alternative starting configurations for 12GDP, and LC3 for 13GDP; see Fig. 2), the simulation duration t and the reference temperature T are reported. A final subscript (1-3) in the label indicates a simulation repeat with different initial velocities. The simulations involve either a glycerol-1,3-dipalmitate (13GDP) or a glycerol-1,2-dipalmitate (12GDP, racemic in each leaflet) bilayer patch of 2×8×8 lipids and are carried out at the reference pressure P = 1 bar. For compactness, a single entry is provided for each set of simulations carried out at different temperatures T (value in Kelvin, sometimes noted generically $\mathcal{T}$ in the simulation label). For example the notation $\mathcal{T} \in \{250-370\}$ indicates a set of seven simulations at temperatures T ranging from 250 to 370 K in steps of 20 K. Note that $D_{12}F_{LC2}350$ and $D_{12}E_{LC}370$ are listed separately from $D_{12}F_{LC2}\mathcal{T}$ and $D_{12}E_{LC}\mathcal{T}$, respectively, because of their different durations.

Simulation	Hydration	n_W	c_W (%w/w)	Starting configuration	t (ns)	T (K)
$P_NF_{GL}318$	F	853	36.3	GL	600	318
$P_NF_{LC}338$	F	853	36.3	GL	600	338
$D_{13}F_{GL}\mathcal{T}$	F	1706	42.2	GL	300	$\mathcal{T} \in \{250--370\}$
$D_{13}F_{LC}\mathcal{T}$	F	1706	42.2	LC	300	$\mathcal{T} \in \{250--370\}$
$D_{13}F_{LC3}\mathcal{T}$	F	1706	42.2	LC3	40	$\mathcal{T} \in \{290--350\}$
$D_{13}F_{GL}370_1$	F	1706	42.2	GL	300	370
$D_{13}F_{GL}370_2$	F	1706	42.2	GL	300	370
$D_{13}F_{GL}370_3$	F	1706	42.2	GL	300	370
$D_{13}F_{LC}370_1$	F	1706	42.2	LC	300	370
$D_{13}F_{LC}370_2$	F	1706	42.2	LC	80	370
$D_{13}F_{LC}370_3$	F	1706	42.2	LC	300	370
$D_{12}F_{GL}\mathcal{T}$	F	1706	42.2	GL	300	$\mathcal{T} \in \{250--370\}$
$D_{12}F_{LC}\mathcal{T}$	F	1706	42.2	LC	300	$\mathcal{T} \in \{250--370\}$
$D_{12}F_{LC1}\mathcal{T}$	F	1706	42.2	LC1	40	$\mathcal{T} \in \{290--350\}$
$D_{12}F_{LC2}\mathcal{T}$	F	1706	42.2	LC2	20	$\mathcal{T} \in \{290--330\}$
$D_{12}F_{LC2}350$	F	1706	42.2	LC2	300	350
$D_{12}F_{GL}370_1$	F	1706	42.2	GL	80	370
$D_{12}F_{GL}370_2$	F	1706	42.2	GL	80	370
$D_{12}F_{GL}370_3$	F	1706	42.2	GL	80	370
$D_{12}F_{LC}370_1$	F	1706	42.2	LC	80	370
$D_{12}F_{LC}370_2$	F	1706	42.2	LC	80	370
$D_{12}F_{LC}370_3$	F	1706	42.2	LC	80	370
$D_{12}E_{GL}\mathcal{T}$	E	2559	63.3	GL	300	$\mathcal{T} \in \{250--370\}$
$D_{12}E_{LC}\mathcal{T}$	E	2559	63.3	LC	300	$\mathcal{T} \in \{250--350\}$
$D_{12}E_{LC}370$	E	2559	63.3	LC	200	370
$D_{12}E_{LC}370_1$	E	2559	63.3	LC	160	370

with different initial velocities were only carried out at 370 K. Simulations at elevated hydration were only performed for the 12GDP system.

In this article, each of the 67 GDP simulations (Table 1) is uniquely identified by a string consisting in sequence of the letters D (GDP system), 13 or 12 (GDP isomer, subscript), F or E (hydration level), GL, LC, LC1, LC2 or LC3 (initial configuration; subscript), followed by the temperature T and, for simulation repeats which differ only by the initial velocities, the repeat index (1-3; subscript). The GMP simulations are labeled as described in Ref. [23], the corresponding labels starting with P_N (GMP system) instead of D_{13} or D_{12}.

The initial structures in GL and LC-like configurations referred to as the original structures were generated from an existing trajectory snapshot of a double-tailed DPPC phospholipid by deletion of the superfluous headgroup atoms followed by energy minimization. The molecule was then replicated on a 2×8×8 lattice to form a bilayer structure with 64 lipids per leaflet. Water molecules were added to the system by random insertion. For 13GDP, the connectivity of the second tail was shifted from the second to the third glycerol carbon atom. For 12GDP, the reference improper-dihedral angle controlling the chirality of the substituted glycerol moiety was set to opposite values for half of the lipid molecules in each leaflet, so as to generate a racemic bilayer. Energy minimization and equilibration at 310 K was followed by heating to 600 K with position constraints on the lipid atoms, in order to allow for faster relaxation of the water molecules, and by a thermalization step to equilibrate the system at a temperature ensuring the stability of either the GL (250 K) or of a LC-like (350 K) phase, carried out in the presence of progressively decreasing position restraints on the lipid atoms.

The initial configuration for the 12GDP systems at elevated hydration was generated from the original structure in the GL phase at full hydration after 300 ns of simulation at 250 K. The appropriate number of water molecules was added to the system. Energy minimization and equilibration during 50 ns at 250 or 370 K provided initial structures representative of the GL and LC-like phases, respectively.

As will be discussed in Section 3, it was difficult to obtain a simulation presenting a stable LC phase for the GDP systems. For this reason, a number of simulations were branched from time points where LC-like structures appeared to present a marginal stability. As shown in Fig. 2, these alternative starting structures for the LC phase, LC1 and LC2 for 12GDP or LC3 for 13GDP, were taken from the runs started from the original LC-like structures and carried out at 370 K (at 4 ns for LC1, 8 ns for LC2, and 300 ns for LC3).

2.3. Trajectory analysis

The simulations were analyzed in terms of the following properties: (*i*) phase-assignment descriptor η; (*ii*) area per lipid a_{xy}; (*iii*) bilayer thickness d_z; (*iv*) volume per lipid v_{xyd}; (*v*) carbon-hydrogen order parameters $S_{CH}(C_n)$ of the 14 methylene groups (n = 2-15) and corresponding chain-averaged value S_{chn}; (*vi*) single-lipid and collective apical tilt angles θ and Θ, respectively, of the acyl chains relative to the bilayer normal; (*vii*) single-lipid and collective azimuthal tilt angles ϕ and Φ, respectively, characterizing the orientation of the lipid head-tail vectors relative to the x-axis; (*viii*) lipid lateral diffusion coefficients D_{xy}.

The procedures employed for the different types of analyses have been described previously [20,22–24] and will not be repeated in details here. The area per lipid a_{xy} was monitored as a function of time, as indicator of a phase transition. The azimuthal tilt angles ϕ and Φ were monitored in the form of time series as well. Averages of all of the other parameters (a_{xy}, d_z, v_{xyd}, S_{chn}, θ, Θ, and D_{xy}) were calculated over the last 24 ns of the simulations, as structural and

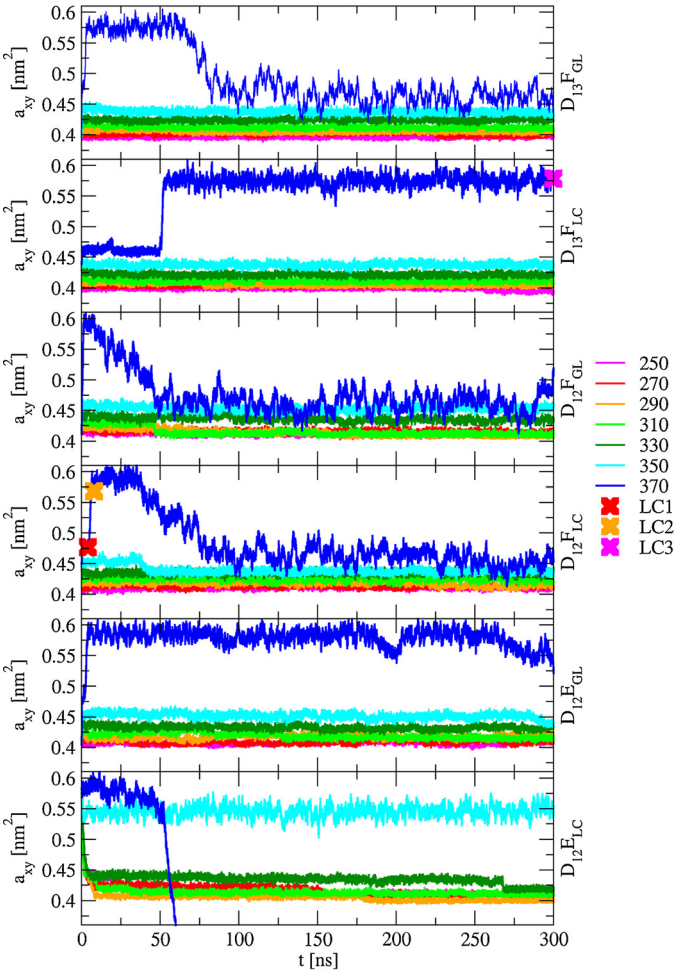

Fig. 2. Time series of the area per lipid along six series of simulations. The simulations differ by the structural isomer (13GDP or 12GDP), the initial structure (GL or LC-like) and the hydration level (F or E). They were started from a structure appropriate for the GL or a LC-like phase and carried out at reference temperatures T ranging from 250 to 370 K (series $D_{13}F_{GL}\mathcal{T}$, $D_{13}F_{LC}\mathcal{T}$, $D_{12}F_{GL}\mathcal{T}$, $D_{12}F_{LC}\mathcal{T}$, $D_{12}E_{GL}\mathcal{T}$ and $D_{12}E_{LC}\mathcal{T}$). The alternative starting structures LC1 and LC2 (for 12GDP) as well as LC3 (for 13GDP) are indicated by crosses. The simulation labels and conditions are summarized in Table 1.

dynamic characteristics of the final phase. For the order parameters $S_{CH}(C_n)$, the methylene group indexes n = 2-15 correspond to atoms 11-24 in Fig. 1 for GMP. For 13GDP, these correspond to atoms 5-18 and 27-40 in the two topologically equivalent chains. For 12GDP these correspond to atoms 8-21 in chain sn2 and 27-40 in chain sn1. To assess a possible difference between the behavior of the two acyl chains, the analyses of $S_{CH}(C_n)$, S_{chn} and θ were performed separately for the two chains. Since no significant difference was found, only average values are normally reported.

The tilt angles are defined as in Ref. [24] (see Fig. 3 therein). They are based on single-lipid head-tail vectors $\mathbf{v}_n$ defined by the ester carbonyl carbon atom and the terminal methyl group of each chain. In a given trajectory configuration, the single-lipid apical tilt angle θ_n is defined as the angle between $\mathbf{v}_n$ and the z-axis of the box (along the bilayer normal, pointing from bottom to top leaflet). This angle spans the range 0-180°, and is typically smaller than 90° for the bottom leaflet and larger than 90° for the top leaflet. The average of the angles θ_n (bottom leaflet) or 180°-θ_n (top leaflet) over all lipids of the bilayer, reported as θ, characterizes the average tilt of the single-lipid head-tail vectors relative to a leaflet-to-midplane axis and is typically smaller than 90°. The single-lipid azimuthal tilt angle ϕ_n is defined as the angle between the projection of $\mathbf{v}_n$

in the *xy*-plane (bilayer plane) and the *x*-axis of the box. This angle spans the range of 0-360°. Averaging the angles ϕ_n over all lipids makes little sense considering that these angles typically span a large fraction of the periodic range 0-360°. Thus these angles are monitored for each lipid separately.

In addition, collective tilt angles are defined separately for the bottom and top leaflets of the bilayer by considering the corresponding vector sums of single-lipid head-tail vectors, $\mathbf{V}_{bot}$ and $\mathbf{V}_{top}$. The collective apical tilt angles Θ_{bot} and Θ_{top} are defined as the angles between $\mathbf{V}_{bot}$ and $\mathbf{V}_{top}$, respectively, and the *z*-axis. The average of Θ_{bot} and 180°-Θ_{top}, reported as Θ, characterizes the extent of collective tilting of the lipids. The collective azimuthal tilt angles Φ_{bot} and Φ_{top} are defined as the angles between the projections of $\mathbf{V}_{bot}$ and $\mathbf{V}_{top}$, respectively, in the *xy*-plane and the *x*-axis. The angles Φ_{bot} and Φ_{top} may present different behaviors [24,25], and are thus monitored separately.

The phase-assignment descriptor η is defined as in Ref. [23] (see Eq. 1 therein), although using slightly different definition parameters in the context of GDP. The idea of this descriptor is to tentatively ascribe a phase to each trajectory configuration, so as to facilitate the monitoring of phase transitions along the trajectories and quantify the extent of sampling of the different phases in a simulation. This single-configuration descriptor η is defined as

$$\eta = \begin{cases} \text{LC} & \text{if } a \geq a_c, h \leq h_c \text{ and } g > g_c \\ \text{GL} & \text{if } a < a_c, h > h_c \text{ and } g > g_c \\ \text{ID} & \text{if } a \geq a'_c, h \leq h'_c \text{ and } g \leq g_c \\ \text{UN} & \text{otherwise} \end{cases} \quad (1)$$

where the different phases are liquid crystal (LC), gel (GL), interdigitated (ID), and unassigned (UN). Here, *a* is the area per lipid (a_{xy}, see above), *h* the headgroup-headgroup distance across the bilayer, and *g* the tail-tail distance across the bilayer. The parameters *h* and *g* are calculated for a trajectory configuration by periodic gathering of the lipid atoms along the *z*-direction with the bilayer midplane (average of the *z*-coordinates of all terminal methyl groups) at $z = 0$, and measurement of the average *z*-distance between the glycerol central carbon atoms (*h*) or the tail methyl united atoms (*g*) of the bottom and top layers, respectively (top minus bottom). Note that *h* is defined here slightly differently from the bilayer thickness (d_z, see above, defined by the *z*-coordinate of the three atoms of the ester group; d_z is typically about 0.6 nm smaller than *h*).

The cutoff values in Eq. 1 were defined by visual inspection of the sampled phases and correlation with their *a*, *h* and *g* values. They are set to $a_c = 0.29\,\text{nm}^2$, $a'_c = 0.35\,\text{nm}^2$, $h_c = 3.9\,\text{nm}$, $h'_c = 2.9\,\text{nm}$ and $g_c = -0.5\,\text{nm}$ for GMP, based on Refs. [23,25,24]. Different values must be used for GDP (to account for the presence of two chains), namely $a_c = 0.50\,\text{nm}^2$, $a'_c = 0.50\,\text{nm}^2$, $h_c = 3.9\,\text{nm}$, $h'_c = 3.9\,\text{nm}$ and $g_c = -0.5\,\text{nm}$. Note that the descriptor assumes a bilayer geometry of the system, and is not intended to provide a reliable assignment for non-bilayer phases. These are usually reported as unassigned (UN), but may sometimes coincidentally meet the conditions for a spurious assignment to a LC, GL or ID phase.

3. Results and discussion

The area per lipid a_{xy} was monitored as a function of time, as an indicator of the phase. The corresponding time evolutions are displayed in Fig. 2 for the six series of seven GDP simulations started from the original GL or LC-like structures and carried out at temperatures in the range 250–370 K (Table 1).

The values characteristic of the GL and LC phases are located in distinct ranges, comparable for both GDP isomers and at the two hydration levels for 12GDP, namely about 0.40–0.45 nm^2 for the GL phase and 0.55–0.60 nm^2 for the LC phase. For the GL phase, observed at the five lowest temperatures (250–330 K) as well as at 350 K (with one exception), a slight temperature dependence of the average a_{xy} value within the above range is observed. The LC phase only occurs at the highest temperature of 370 K as well as once at 350 K, and shows larger fluctuations in a_{xy}. However, this phase is only stable for a significant amount of time and still present at the end of the 300 ns time period in three cases. These are simulations $D_{13}F_{LC}370$, $D_{12}E_{LC}350$ and $D_{12}E_{GL}370$. Note that in simulation $D_{12}E_{GL}370$, the onset of a transition appears at the very end of the simulation (see the end of the corresponding a_{xy} curve in Fig. 2). In all other cases, after a short period in the LC phase, the bilayer undergoes a transition to a non-bilayer phase, visible as a sudden decrease in a_{xy} (which then no longer corresponds to an area per lipid). This phase is either an inverted-cylinder phase (Fig. 3, bottom middle and right panels), only observed at full hydration and with an apparent a_{xy} value of about 0.45–0.50 nm^2, or a stacked phase (Fig. 3, bottom left panel), only observed at elevated hydration and with a significantly smaller apparent a_{xy} value.

The phase-transition behavior for the entire set of 67 simulations is summarized in Table 2 on the basis of the phase-assignment descriptor η. The descriptor was able to distinguish correctly between the different phases, except in four cases (corrected in the table): in simulations $D_{13}F_{LC}370_2$ and $D_{12}F_{LC}370_3$, the descriptor returned LC although the system was in an inverted-cylinder phase, and in simulations $D_{12}E_{LC}370_1$ and $D_{12}E_{LC}370$, the descriptor returned GL, although the system was in a stacked phase. This is because the descriptor assumes a bilayer geometry of the system and is not intended to provide a reliable assignment for non-bilayer phases, which may sometimes coincidentally meet the conditions for a spurious assignment to one of the bilayer phases. In all other cases, the descriptor correctly returned UN (unassigned) for non-bilayer phases. All simulations evidenced no, one (GL→LC, LC→GL or LC→UN), or two (GL→LC→UN) phase transitions. For the simulations sampling transiently (for at least 5 ns) the LC phase, the time spent in this phase is also indicated between parentheses in the table.

For 13GDP, upon starting from the original LC-like configuration (simulations $D_{13}F_{LC}\mathcal{T}$ with $\mathcal{T} \in \{250–370\}$), a stable LC phase is only observed at 370 K (simulation $D_{13}F_{LC}370$), albeit with a much higher area per lipid compared to this initial configuration (Fig. 2). This indicates that the original LC-like structure was probably not sufficiently equilibrated. For this reason, the final structure of simulation $D_{13}F_{LC}370$, labeled LC3, was used to branch a new set of simulations at lower temperatures (simulations $D_{13}F_{LC3}\mathcal{T}$ with $\mathcal{T} \in \{290–350\}$). All these simulations result in a LC→GL transition within at most 40 ns. Among three repeats of $D_{13}F_{GL}370$ and $D_{13}F_{LC}370$, two also present a stable LC phase, the four others leading to GL or UN phases. Irrespective of the starting structure, all simulations of 13GDP carried out at temperatures of 350 K or below lead to a stable GL phase.

For 12 GDP at full hydration, no stable LC phase is observed upon starting from the original GL or LC-like configurations (simulations $D_{12}F_{GL}\mathcal{T}$ and $D_{12}F_{LC}\mathcal{T}$ with $\mathcal{T} \in \{250 - 370\}$). As a first attempt to obtain a stable LC phase, configuration LC1 (at 4 ns in simulation $D_{12}F_{LC}370$) was used to branch a new set of simulations ($D_{12}F_{LC1}\mathcal{T}$ with $\mathcal{T} \in \{290–350\}$), none of which result in a stable LC phase. As a second attempt, configuration LC2 (at 8 ns in simulation $D_{12}F_{LC}370$) was also used to branch a new set of simulations ($D_{12}F_{LC2}\mathcal{T}$ with $\mathcal{T} \in \{290–350\}$), none of which result in a stable LC phase either. One of them, $D_{12}F_{LC2}350$, stays in the LC phase for 294 ns before undergoing a transition to an inverted-cylinder phase. Finally, among three repeats of $D_{12}F_{GL}370$ and $D_{12}F_{LC}370$, none adopt a stable LC phase. In summary, irrespective of the starting structure, none of the 12GDP simulations carried out at full hydration in the temperature range 250–370 K leads to a stable LC phase.

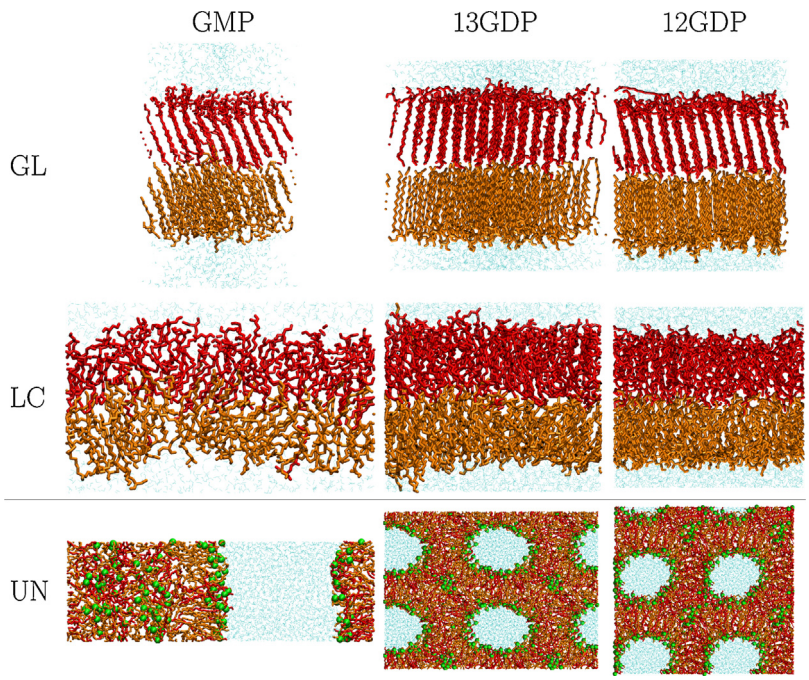

Fig. 3. Illustrative structures corresponding to the different phases of the GMP and GDP lipid systems. Top and middle: snapshots illustrating the GL and LC phases for GMP (simulation $M_EF_{GL}310$ of Ref. [23] at 60 and 240 ns, respectively), for 13GDP (simulations $D_{13}F_{GL}310$ and $D_{13}F_{LC}370_1$, both at 300 ns) and 12GDP (simulations $D_{12}F_{GL}310$ at 300 ns and $D_{12}F_{LC2}350$ at 200 ns). Bottom right: for the two GDP isomers, illustrative structures for the inverted-cylinder phase (simulations $D_{13}F_{LC}370$ and $D_{12}F_{LC}370$, both at 300 ns). Bottom left: for 12GDP, illustrative structure for the stacked phase (simulation $D_{12}E_{LC}370$ at 300 ns). Water molecules are displayed in light blue. For the two inverted-cylinder snapshots, four periodic copies are shown to highlight the tubular structure. In the three bottom structures, the glycerol central carbon atom (atoms 20 and 4 for 13GDP and 12GDP, respectively, in Fig. 1) are shown as green balls to indicate the position of the headgroups. All structures are shown along the *x*-axis of the box with the *z*-axis vertical, except the structures for GL, which were rotated around the *z*-axis to highlight their structural characteristics, and the structure for the stacked phase, which is shown with the *z*-axis horizontal. The simulation labels and conditions are summarized in Table 1.

Table 2
Final phases for the entire set of simulations. Shown are the final phase (GL for gel, LC for liquid crystal or UN for non-bilayer phases; Fig. 3) of the different simulations depending on the starting configuration (GL, LC, LC1, LC2 or LC3; Fig. 2), the hydration level (full hydration in all cases except 12GDP(E) involving an elevated water content) and the simulation temperature *T*. The UN phase is either an inverted-cylinder (full hydration) or a stacked (elevated hydration) phase. For the simulations sampling transiently (for at least 5 ns) the LC phase, the time spent in this phase is also indicated between parentheses (in units of ns). Although simulation $D_{12}E_{GL}370$ ends in the LC phase, the onset of a transition appears at the very end of the simulation (see the end of the corresponding a_{xy} curve in Fig. 2), reason for which the corresponding entry is between parentheses. For comparison, for GMP, the highest temperature leading to a stable GL phase and the lowest temperature leading to a stable LC phase are also indicated (data from Ref. [23] at full hydration). Note that all occurrences of UN were reached *via* the LC phase. See Table 1 for the simulation labels and conditions.

T (K)	Initial phase									
	GMP	13GDP			12GDP				12GDP(E)	
		GL	LC	LC3	GL	LC	LC1	LC2	GL	LC
250		GL	GL		GL	GL			GL	GL
270		GL	GL		GL	GL			GL	GL
290		GL	GL	GL	GL	GL	GL	GL	GL	GL
310		GL	GL	GL	GL	GL	GL	GL	GL	GL
318	GL									
322	LC									
330		GL	GL	GL	GL	GL	GL	GL	GL	GL
350		GL	GL	GL	GL	GL	GL	UN(279)	GL	LC
370		UN(77)	LC		UN(27)	UN(48)			(LC)	UN(52)
370(1)		LC	LC		UN(12)	UN(43)				UN(175)
370(2)		UN(136)	GL		UN(30)	UN(45)				
370(3)		UN(139)	UN(24)		UN(13)	UN(41)				

Observing that most simulations aiming at obtaining a stable LC phase result in an inverted-cylinder phase, where water is trapped within a lipid matrix, the possibility was envisioned that the phase behavior could be influenced by the hydration level. For this reason, the simulations of 12 GDP starting from the original GL or LC-like configurations were repeated with extended hydration (simulations $D_{12}E_{GL}\mathcal{T}$ and $D_{12}E_{LC}\mathcal{T}$ with $\mathcal{T}\in\{250–370\}$). In this case, two simulations ($D_{12}E_{LC}350$ and $D_{12}E_{GL}370$) result in a stable LC phase. This phase is again characterized by a much higher area per lipid compared to the original LC-like or the alternative LC1 configurations (but comparable to the LC2 structure), indicating that these two structures were not sufficiently equilibrated. Except for $D_{12}E_{LC}350$, the GL phase is stable in all simulations carried out at 350 K or below.

In summary, although nearly all simulations evidence a stable GL phase for both 13GDP and 12GDP at temperatures of 350 K or below, only three simulations of 13GDP at full hydration ($D_{13}F_{LC}370$, $D_{13}F_{GL}370_1$ and $D_{13}F_{LC}370_1$) and two simulations of 12GDP at extended hydration ($D_{12}E_{LC}350$ and $D_{13}E_{GL}370$) present a LC phase stable at least over 300 ns, at either 350 or 370 K. This suggests

a T_m of about 350 K for both GDP isomers, close to the experimental T_m values [56–58] of 72–74°C (about 346 K) for 13GDP and 63-66°C (about 338 K) for 12GDP, and significantly higher than the corresponding value [43] of 50°C (about 323 K) for GMP. The experimental numbers suggest a slightly higher stability of the LC phase for 12GDP compared to 13 GDP, but the simulation results (including the effect of hydration) are too ambiguous for evidencing clearly such a trend.

Illustrative structures for the different phases encountered in the simulations are shown in Fig. 3 for the two GDP isomers, along with corresponding structures for GMP from Ref. [23]. In the GL phase, the lipids are aligned, the tails present nearly all-*trans* dihedral conformations, and they are tilted relative to the bilayer normal. As apparent from the structures, the tilt angle is reduced for GDP compared to GMP (see further below). In comparison to the GL phase, the LC phase is disordered, with no lipid alignment, and the tails present tilts and kinks in uncorrelated directions. As mentioned above, the GDP systems can undergo a massive structural change to non-bilayer configurations at high temperatures ($T \geq 350$ K). At full hydration, for both isomers, an inverted-cylinder phase can be formed, where water is confined to a small region surrounded by lipid headgroups. This inverted-cylinder phase is similar to an inverted-hexagonal phase [73], except for the occurrence of lipids oriented away from the water cylinders and the presence of a small number of water molecules among the lipid tails (hydrated headgroup clusters in the hydrophobic region). At elevated hydration (considered for 12GDP only), a stacked arrangement is observed, where a planar water layer is coated by headgroups. However, the tail region does not consist of a single bilayer, but also encompasses some headgroups along with a number of water molecules. The formation of such non-bilayer or inverted structures at high temperatures has been observed experimentally in many diglyceride-rich lipid systems, as reviewed in Ref. [54].

The main structural and dynamic properties of the GL and LC phases of GMP, 13GDP and 12 GDP are reported in Table 3. The values for GDP are taken from representative simulations with a stable GL phase (at 310 K) or LC phase (at 350 or 370 K). The values for GMP are taken from Ref. [23] and correspond to 318 and 338 K, respectively. The values for the entire set of simulations can be found in Tables S.1 and S.2 of the supplementary material document.

As expected, the area per lipid presents a substantial increase from GMP to GDP, due to the presence of two aliphatic tails instead of one. However, the values for both the GL and LC phases are smaller (by about 15%) than twice those of GMP. This is not surprising, considering that although the number of tails has doubled, the extent of collective (GL) or single-lipid (LC) tilting has significantly decreased. For GMP, the single-lipid and collective tilt angles in the GL phase are $\theta \approx 20°$ and $\Theta \approx 15°$, respectively, while the single-lipid tilt angle in the LC phase is $\theta \approx 30°$. For the GDP isomers, these values are reduced by about 5–10°. This decrease of the tilt angle is caused by a reduction of the mismatch between headgroup and tail cross-sections [24] in GDP (two tails) compared to GMP (one tail). Note that the GL phase of 12GDP is experimentally known to be tilted [53,74].

The bilayer thickness d_z for the GDP isomers is about 4.2 nm in the GL phase, qualitatively comparable to the experimental estimate [75] of 4.3 nm for DPPC in the GL phase at 20°C. Note that the close similarity between the two numbers is in part coincidental, arising from the compensation between two factors. The thickness for DPPC (based on an electron density profile) is increased by the presence of the choline headgroup, while the thickness for GDP is increased due to the lower tilt angle. The corresponding value for the LC phase is about 3.3 nm. In both phases, d_z is about 10% larger compared to GMP, which is in line with the reduction of the (single-lipid or collective) tilt angle. The chain-averaged order

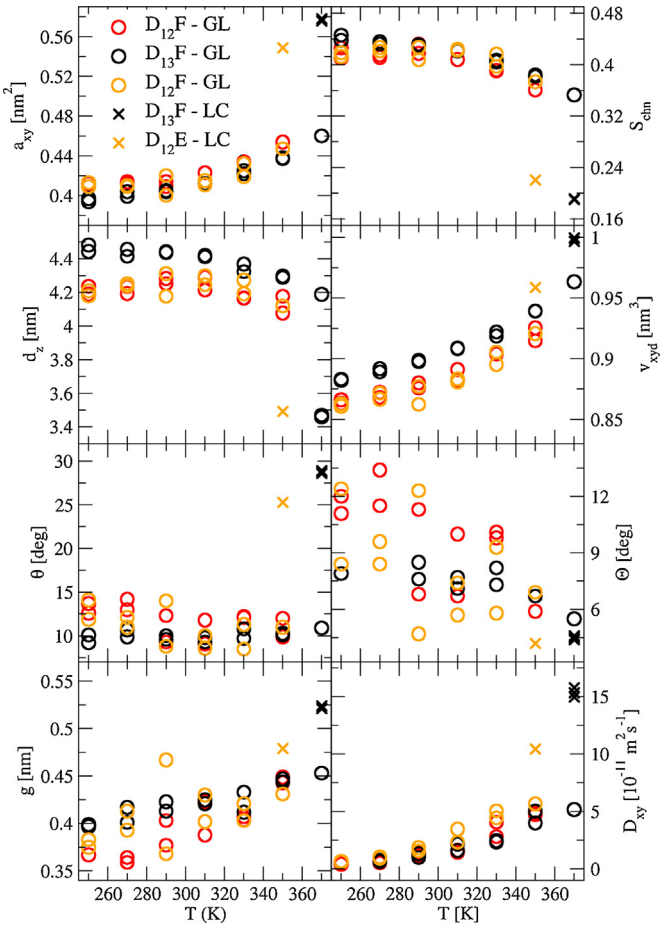

Fig. 4. Temperature and phase dependence of bilayer structural parameters for the GL and LC phases. Shown as a function of the temperature T are the area per lipid a_{xy}, the chain-averaged order parameter S_{chn}, the bilayer thickness d_z, the volume per lipid v_{xyd}, the single-lipid and collective tilt angles θ and Θ, respectively, the tail-tail distance g (reference point: terminal methyl group), and the lateral diffusion coefficient D_{xy}. The values are averaged over the last 24 ns of the simulations. The simulations differ by the structural isomer (12GDP or 13GDP), the hydration level (F or E), and the final phase of the simulation (GL or LC, indicated by the symbol). They were started from a structure appropriate for GL or LC-like phases and carried out at reference temperatures ranging from 250 to 370 K. Only simulations resulting in a stable GL or LC phase are considered (no non-bilayer structures; simulation $D_{12}E_{LC}370$ is also excluded). The values for GDP are averaged over the two chains. The simulation labels and conditions are summarized in Table 1. The corresponding data can be found numerically in Tables S.2 and S.1 of the supplementary material document.

parameters S_{chn} for the GDP isomers are higher than those of GMP in both phases, especially in the GL phase. This may be due in part to the higher extent of ordering, but also to the smaller tilt angles [76].

In terms of dynamic properties, the lateral diffusion constant D_{xy} is reduced by about a factor two in the GL phase, whereas it is not significantly affected in the LC phase. Comparison of the estimates of about 15.0 and 10.5×10^{-11} m^{2}s^{-1} for 13GDP and 12GDP, respectively, in the LC phase with the experimental [77] and simulation [40] values of 1.25 and 0.95×10^{-11} m^{2}s^{-1}, respectively, for DPPC at 50° indicates that the lateral diffusion of GDP molecules (low polarity headgroup) is much more rapid than that of DPPC molecules (zwitterionic headgroup).

The dependence of selected structural parameters on temperature and phase for simulations started from GL or LC-like structures and which resulted in stable GL or LC phases is shown in Fig. 4. In the GL phase, the area per lipid a_{xy} and chain-averaged order parameter S_{chn} are similar for both isomers and hydration levels,

Table 3
Structural and dynamic properties of the GL and LC phases for a subset of simulations. The data for GMP is taken from Ref. [23] (simulations $P_NF_{GL}318$ and $P_NF_{LC}338$ therein). For 13GDP, simulations $D_{13}F_{GL}310$ and $D_{13}F_{LC}370$, and for 12GDP, simulations $D_{12}F_{GL}310$ and $D_{12}E_{LC}350$ are selected as references for the GL and LC phases, respectively. The reported quantities, averaged over the last 24 ns of the simulations, are the area per lipid a_{xy}, the chain-averaged order parameter S_{chn}, the bilayer thickness d_z, the volume per lipid v_{xyd}, the single-lipid and collective tilt angles θ and Θ, respectively, the headgroup-headgroup distance h (reference point: glycerol central carbon atom) and the tail-tail distance g (reference point: terminal methyl group) across the bilayer, and the lateral diffusion coefficient D_{xy}. The values for GDP are averaged over the two chains. See Table 1 for simulation labels and conditions. Corresponding data for the entire set of 67 simulations can be found in Tables S.1 and S.2 of the supplementary material document.

	GL			LC		
	GMP	13GDP	12GDP	GMP	13GDP	12GDP
a_{xy} [nm^2]	0.243	0.411	0.411	0.328	0.576	0.549
S_{chn}	0.305	0.423	0.423	0.152	0.191	0.220
d_z [nm]	4.00	4.24	4.21	3.09	3.32	3.32
v_{xyd} [nm^3]	0.46	0.87	0.86	0.48	0.95	0.91
θ [deg]	20.5	9.3	9.1	32.4	28.6	25.3
Θ [deg]	15.0	7.1	6.7	7.0	4.4	4.4
h [nm]	4.14	4.42	4.29	3.31	3.47	3.49
g [nm]	0.42	0.43	0.42	0.36	0.52	0.48
D_{xy} [10^{-11} m^{2}s^{-1}]	3.0	1.6	1.4	13.8	15.0	10.5

but the bilayer thickness d_z and the volume per lipid v_{xyd} present slightly higher values for 13GDP. This is accompanied by tendentially lower values of the single-lipid and collective tilt angles θ and Θ, respectively. An exception to this trend is the lower values of Θ for the simulations of the $D_{12}E$ series. In this phase, a_{xy}, v_{xyd} and D_{xy} evidence a slight increase, and S_{chn}, d_z and Θ a slight decrease upon increasing the temperature, with θ being essentially temperature independent. These changes result from the enhanced thermal motion and mobility at higher temperature, which induces a lateral expansion of the bilayer. In turn, the increase in a_{xy} affects all the other parameters, the correlations being qualitatively similar to those previously observed for GMP in Ref. [23] (see Fig. 7 therein). Note, however, that in the case of GMP, these correlations were most evident for the LC rather than the GL phase. The observation of clear trends in the GL phase for GDP is certainly in part due to the larger temperature interval considered here (270–350 K *vs.* 318–338 K in the GMP study [23]), but probably also results from a higher plasticity of the GL phase of GMP compared to GDP.

Considering the LC phase, only four data points are represented in Fig. 4. The final configuration of simulation $D_{12}E_{LC}370$ was excluded because its structural parameters suggest the onset of a transition to a non-bilayer phase (see the end of the corresponding a_{xy} curve in Fig. 2 and the structural parameters in supplementary material Table S.2). This limited set only permits qualitative observations to be made, considering that the data for 12GDP and 13GDP correspond to two different temperatures. Nevertheless, it appears that 13GDP presents slightly higher a_{xy}, θ and D_{xy}, a comparable d_z, and lower S_{chn} compared to 12GDP in the LC phase, suggesting a higher extent of disorder and mobility.

The carbon-hydrogen order parameters $S_{CH}(C_n)$ of the 14 methylene groups are displayed as a function of the carbon atom number (n = 2-15) in Fig. 5 for illustrative systems representative of the GL

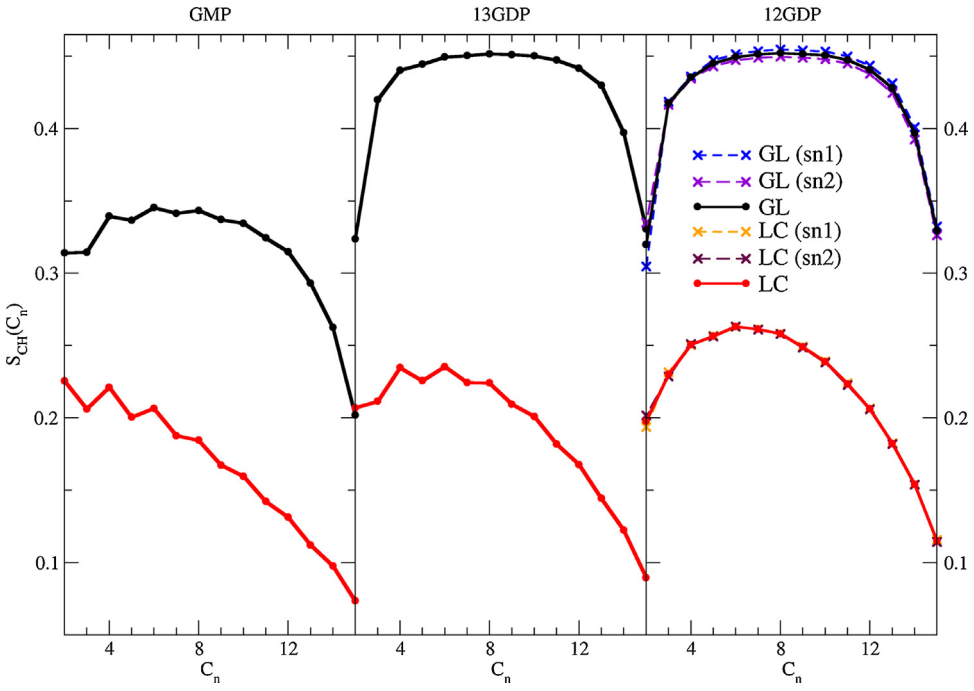

Fig. 5. Carbon-hydrogen order parameters of the 14 methylene groups. Shown are the order parameters $S_{CH}(C_n)$ as a function of the carbon atom number C_n (n = 2-15) for illustrative simulations of GMP, 13GDP and 12GDP in the GL or LC phase. Note that the lines are only meant as guide for the eye. The data for GMP is taken from Ref. [23] (simulations $P_NF_{GL}318$ and $P_NF_{LC}338$ therein). Simulations $D_{13}F_{GL}310$ and $D_{13}F_{LC}370$ for 13GDP, and simulations $D_{12}F_{GL}310$ and $D_{12}E_{LC}350$ for 12GDP are selected as references for the GL and LC phases, respectively. The data is averaged over the last 24 ns of the simulations. The values for GDP are averaged over the two chains. For 12GDP, the values for the topologically distinct chains sn1 and sn2 are also displayed separately. The simulation labels and conditions are summarized in Table 1.

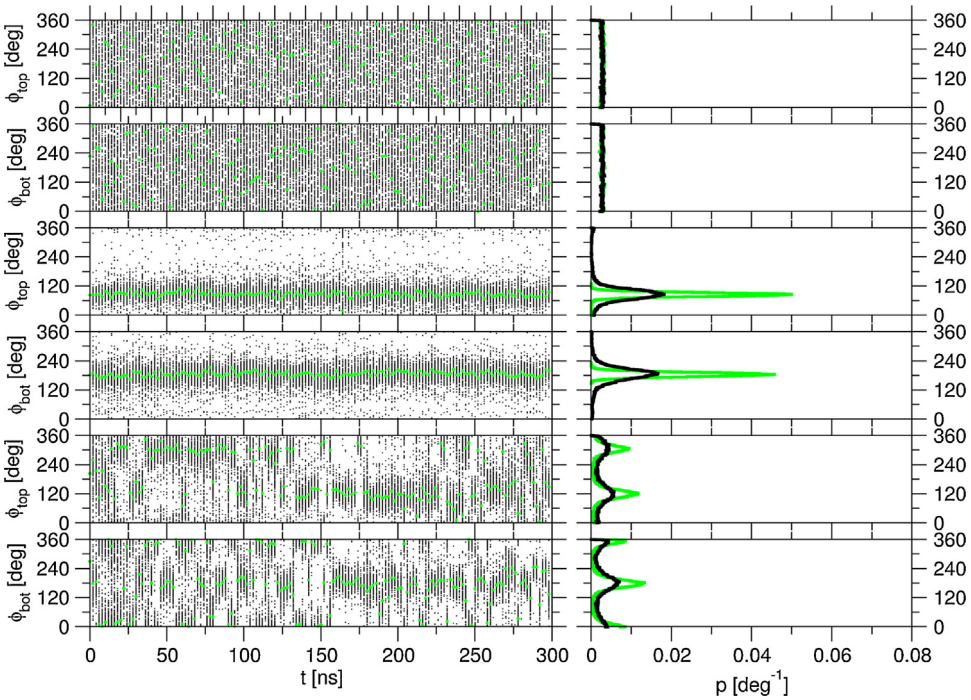

Fig. 6. Illustrative azimuthal tilt angle trajectories and probability distributions for the GL and LC phases. Shown are the azimuthal tilt angle values ϕ_n for each individual lipid n (black dots) and the collective value Φ (green dots) along with their probability distributions (black and green curves), separately for the top and bottom leaflets. From top to bottom, simulations $D_{12}F_{LC2}350$ (LC phase, transition to a non-bilayer phase at 279 ns), $D_{12}F_{GL}250$ (GL phase, no tilt precession) and $D_{12}E_{LC}330$ (GL phase, with tilt precession) are considered. The simulation labels and conditions are summarized in Table 1.

and LC phases of GMP, 13GDP and 12GDP. For 12GDP, the values for the topologically distinct chains sn1 and sn2 are also displayed separately but present marginal differences, so that only their average is considered here. For the three lipids, the values for the GL phase are higher than those for the LC phase. The order parameters for the GL phase are also significantly higher for both GDP isomers compared to GMP. This indicates a more ordered tail region for GDP due to the tighter packing caused by two chains, but also reflects in part the lower tilt angle. The order parameters for the LC phase are in similar ranges for the three lipids, with an extent of ordering slightly increasing along the sequence GMP, 13GDP and 12GDP.

For both phases, the order parameters tend to be low for the first two to three carbon atoms, and then decrease along the aliphatic tail, either abruptly (LC phase) or after a long plateau (GL phase). Another prominent feature in Fig. 5 is the zig–zag pattern of the order parameters in the vicinity of the headgroup, pronounced for GMP in both phases and for 13GDP in the LC phase. A similar pattern has been reported previously as the odd-even effect in the context of carbon order parameters S_{CC} for DPPC [76] and other lipids [78,79]. This effect was explained there as resulting from chain tilting in an all-*trans* conformation, but subsequent simulations of GMP suggest alternating dihedral-angle flexibilities as another contributing factor [24].

Illustrative results for the time evolution of the single-lipid azimuthal tilt angles ϕ_n, which characterize the orientation of the lipid head-tail vectors relative to one of the transverse directions (x-axis), are shown in Fig. 6 for illustrative simulations of GDP in the LC and in the GL (two examples) phases. The behavior of the azimuthal tilt angles was previously investigated [24] in the case of GMP, where a tilt precession could be observed in the GL phase. For GDP in the present simulations, a similar precession motion can be seen in many simulations (see example in Fig. 6 bottom). Three main observations made previously in the context of GMP are unaltered for GDP, namely: (*i*) the behavior of the ϕ_n angles is essentially uncorrelated in the LC phase but largely collective in the GL phase, with well-defined alternative orientational states; (*ii*) the bottom and top leaflets may present distinct preferential states, with a possible precession between these states on the 50–100 ns timescale; (*iii*) there is a limited extent of correlation between the preferential states and possible precession motions of the two leaflets. The probabilities of the preferential orientational states in the collective azimuthal tilt angle Φ are reported numerically in the supplementary material document, Tables S.3 and S.4 (bottom layer) or S.5 and S.6 (top layer), for all simulations ending in the GL phase. In this phase, the bottom layer predominantly adopts collective azimuthal orientations of +30° or −150° for 12GDP, and −120° for 13GDP, whereas the top layer shows preferential values of +90° for 12GDP, and +90° or +120° for 13GDP. Because the two leaflets of the bilayer are equivalent (no chirality for 13GDP, racemic mixture for 12GDP), there is no topological distinction between them and between $+\Phi$ and $-\Phi$ values. Thus, one would in principle expect both leaflets to be affected by the same type of preferences, and the distinction only results from the finite sampling time (dependence on the initial structure).

4. Conclusion

The goal of the present study was to investigate the influence of introducing a second aliphatic lipid tail on the phase- and phase-transition properties of GMP lipid bilayers, *i.e.* comparing these properties to those of the diglyceride GDP. To this purpose, a set 67 simulations (up to 300 ns) of $2\times8\times8$ GDP bilayer patches were performed, considering the two isomers 12GDP (racemic) and 13GDP, two hydration levels (12GDP only), and temperatures in the range 250–370 K.

The main results of the simulations are easily rationalized considering two key changes in molecular properties when going from GMP to GDP. First, the functionalization of an additional hydroxyl group of glycerol reduces the headgroup polarity of the molecule. Whereas GMP has two headgroup hydroxyl groups exposed to the

solvent (one per tail), GDP has only one (one half per tail). Second, the introduction of an additional aliphatic tail changes the overall shape of the molecule. Whereas GMP is characterized by a tail cross-section that is too small for its (hydrated) headgroup cross-section [23,24], GDP is wedge-shaped [73] in the opposite direction. Here, the tail cross-section is larger than the headgroup cross-section, also considering the reduced polarity (and thus hydration volume) of the latter.

These features explain why the LC phase of GDP is destabilized relative to that of GMP. Compared to the GL phase, the LC phase involves a larger headgroup spacing and a more extensive hydration, both changes being favorable for GMP and unfavorable for GDP. This causes the increase in T_m observed in the simulations, from about 325 K for GMP to about 350 K for GDP, in qualitative agreement with the experimental values [43,56–58] of 323 K for GMP *vs.* about 346 and 338 K for 13GDP and 12GDP, respectively.

Considering the relative instability of the LC phase of GDP, it is not surprising to observe the occurrence of alternative phases at high temperatures, such as those shown in Fig. 3 (bottom panels). In the inverted-cylinder phase, the appearance of a negatively-curved interface to water is compatible with the wedge shape of the GDP molecule. In both this and the stacked phase, the presence of headgroups in the tail region is also facilitated by the low polarity of the GDP headgroup. Experimentally, the occurrence such non-bilayer or inverted structures is indeed common in diglyceride-rich lipid systems, as reviewed in Ref. [54].

In the simulations, the LC phase becomes tendentially more stable relative to the non-bilayer phases upon increasing the hydration level beyond what is referred to as full hydration in Section 2.1 (and is arguably already a hydration excess for GDP). Note that there is no inconsistency here, as the term full hydration refers to the number of water molecules presenting significant interactions with the lipids in a bilayer phase (and thus affecting the properties of this phase). The relative stabilities of non-bilayer phases are likely to depend in a much more complicated fashion on the lipid-water ratio of the system. Thus, the change in the relative stability of the LC phase when adding water beyond the bilayer full-hydration regime is probably not due to the influence of the extra water on the stability of this phase, but on that of the alternative non-bilayer phases.

Finally, the distinct molecular features of GDP compared to GMP have a significant influence on the structural and dynamic properties of the GL and LC phases. The reduced headgroup size and hydration induces pressure towards tighter chain packing. As a result, the area per lipid is less than twice that of GMP in the two phases (by about 15%), the extent of single-lipid (and collective for the GL phase) tilting is reduced (by about 5-10°), the order parameters are noticeably higher in the GL phase, and the lateral diffusion constant is reduced.

No dramatic differences were found in terms of the phase- and phase-transition properties of the two GDP isomers. In particular, the experimental difference of about 10 K is too small to be detected by the relatively crude T_m estimates derived from the present simulations. The experimental numbers suggest a slightly higher stability of the LC phase for 12GDP compared to 13GDP. This is qualitatively compatible with the observation that the LC phase of 13GDP presents slightly higher area per lipid, tilt angle and lateral diffusion constant compared to 12GDP, along with lower order parameters, suggesting a higher extent of disorder and mobility.

The lack of stability of the LC phase and the occurrence of alternative non-bilayer phases is compatible with the observation that unfunctionalized diglycerides have not been retained by nature as a major component of cell membranes, although they fulfill various biological functions as minor components [53–56]. The functionalization of diglycerides by large or/and polar headgroups leading to molecules such as DPPC certainly serves at least in part to alleviate the wedge-shape/low-polarity properties of GDP, rendering it more apt to forming stable bilayers in the LC phase at physiological temperatures. In this respect, it is interesting to note that the simulation value of about 7° for the collective tilt angle of GDP in the GL phase is substantially lower than the experimentally inferred estimate [80] of 21.5° for DPPC in this phase, similar values being reported in simulations [81,82]. This supports the idea that the headgroup substitution of DPPC indeed makes a decisive difference regarding the tilting of the GL phase and the stability of the LC phase.

Following similar considerations, one may extrapolate the trends observed from GMP to GDP towards triglycerides. Considering the further enhancement of the wedge shape and the near suppression of the headgroup polarity, it is not surprising that the latter compounds do not even form bilayers at all.

Acknowledgements

Financial support from the Swiss National Foundation (grants 21-132739 and 21-138020) is gratefully acknowledged.

Appendix A. Supplementary Data

Supplementary data associated with this article can be found, in the online version, at http://dx.doi.org/10.1016/j.jmgm.2015.04.012

References

[1] G.M. Cooper, R.E. Hausman, The Cell: A Molecular Approach, ASM Press, Washington, DC, USA, 2007.
[2] J.M. Seddon, G. Cevc, Lipid polymorphism: Structure and stability of lyotropic mesophases of phospholipids, in: G. Cevc (Ed.), Phospholipids Handbook;, Marcel Dekker, Inc., New York, USA, 1993, pp. 403–454.
[3] I. Foubert, K. Dewettinck, D. van de Walle, A.J. Dijkstra, P.J. Quinn, Physical properties: Structural and physical characteristic, in: F.D. Gunstone, J.L. Harwood, A.J. Dijkstra (Eds.), The lipid handbook, 3rd ed., CRC Press, Div. of Taylor, Francis Group, Boca Raton, USA, 2007, pp. 471–534.
[4] J.F. Nagle, S. Tristram-Nagle, Structure of lipid bilayers, Biochim. Biophys. Acta 1469 (2000) 159–195.
[5] S.-J. Marrink, O. Berger, P. Tieleman, F. Jähnig, Adhesion forces of lipids in a phospholipid membrane studied by molecular dynamics simulations, Biophys. J. 74 (1998) 931–943.
[6] E. Lindahl, O. Edholm, Spatial and energetic-entropic decomposition of surface tension in lipid bilayers from molecular dynamics simulations, J. Chem. Phys. 113 (2000) 3882–3893.
[7] B.W. Lee, R. Faller, A.K. Sum, I. Vattulainen, M. Patra, M. Karttunen, Structural effects of small molecules on phospholipid bilayers investigated by molecular simulations, Fluid Phase Equilib. 225 (2004) 63–68.
[8] C.S. Pereira, R.D. Lins, I. Chandrasekhar, L.C.G. Freitas, P.H. Hünenberger, Interaction of the disaccharide trehalose with a phospholipid bilayer: a molecular dynamics study, Biophys. J. 86 (2004) 2273–2285.
[9] B.W. Lee, R. Faller, A.K. Sum, I. Vattulainen, M. Patra, M. Karttunen, Structural effects of small molecules on phospholipid bilayers inverstigated by molecular simulations, Fluid Phase Equilib. 228 (2005) 135–140.
[10] A. Skibinsky, R.M. Venable, R.W. Pastor, A molecular dynamics study of the response of lipid bilayers and monolayers to trehalose, Biophys. J. 89 (2005) 4111–4121.
[11] A.M. Massari, I.J. Finkelstein, B.L. McClain, A. Goj, X. Wen, K.L. Bren, R.F. Loring, M.D. Fayer, The influence of aqueous versus glassy solvents on protein dynamics: vibrational echo experiments and molecular dynamics simulations, J. Am. Chem. Soc. 127 (2005) 14279–14289.
[12] J. Chanda, S. Bandyopadhyay, Perturbation of phospholipid bilayer properties by ethanol at a high concentration, Langmuir 22 (2006) 3775–3781.
[13] M. Patra, E. Salonen, E. Terama, I. Vattulainen, R. Faller, B.W. Lee, J. Holopainen, M. Karttunen, Under the influence of alcohol: the effect of ethanol and methanol on lipid bilayers, Biophys. J. 90 (2006) 1121–1135.
[14] V. Knecht, S.-J. Marrink, Molecular dynamics simulations of lipid vesicle fusion in atomic detail, Biophys. J. 92 (2007) 4254–4261.
[15] J.L. MacCallum, D.P. Tieleman, Interactions between small molecules and lipid bilayers, Curr. Top. Membr. 60 (2008) 227–256.
[16] C.S. Pereira, P.H. Hünenberger, The influence of polyhydroxylated compounds on a hydrated phospholipid bilayer: a molecular dynamics study, Mol. Simul. 34 (2008) 403–420.
[17] B.A.C. Horta, L. Perić-Hassler, P.H. Hünenberger, Interaction of the disaccharides trehalose and gentiobiose with lipid bilayers: a comparative molecular dynamics study, J. Mol. Graph. Model 29 (2010) 331–346.

[18] A.P. Lyubartsev, A.L. Rabinovich, Recent development in computer simulation of lipid bilayers, Soft Matter 7 (2011) 25–39.
[19] H. Saito, W. Shinoda, Cholesterol effect on water permeability through DPPC and PSM lipid bilayers: a molecular dynamics study, J. Phys. Chem. B 115 (2011) 15241–15250.
[20] B.A.C. Horta, A.H. de Vries, P.H. Hünenberger, Simulating the transition between gel and liquid-crystal phases of lipid bilayers: dependence of the transition temperature on the hydration level, J. Chem. Theory Comput. 6 (2010) 2488–2500.
[21] B.A.C. Horta, P.H. Hünenberger, Enantiomeric segregation in the gel phase of lipid bilayers, J. Am. Chem. Soc. 133 (2011) 8464–8466.
[22] M. Laner, B.A.C. Horta, P.H. Hünenberger, Phase-transition properties of glycerol-monopalmitate lipid bilayers investigated by molecular dynamics simulation: influence of the system size and force-field parameters, Mol. Simul. 39 (2013) 563–583.
[23] M. Laner, B.A.C. Horta, P.H. Hünenberger, Effect of the cosolutes trehalose and methanol on the equilibrium and phase-transition properties of glycerol-monopalmitate lipid bilayers investigated using molecular dynamics simulations, Eur. Biophys. J. 43 (2014) 517–544.
[24] M. Laner, B.A.C. Horta, P.H. Hünenberger, Long-timescale motions in glycerol-monopalmitate lipid bilayers investigated using molecular dynamics simulation, J. Mol. Graph. Model 55 (2015) 48–64.
[25] M. Laner, P.H. Hünenberger, Effect of methanol on the phase-transition properties of glycerol-monopalmitate lipid bilayers investigated using molecular dynamics simulations: in quest of the biphasic effect, J. Mol. Graph. Model 55 (2015) 85–104.
[26] M. Laner, P.H. Hünenberger, Thermodynamics and kinetics of the gel to liquid-crystal phase transitions in glycerol-monopalmitate lipid bilayers: a Markov model analysis based on atomistic molecular dynamics simulations, 2015 (submitted for publication).
[27] C. Anézo, A.H. de Vries, H.-D. Höltje, D.P. Tieleman, S.-J. Marrink, Methodological issues in lipid bilayer simulations, J. Phys. Chem. B 107 (2003) 9424–9433.
[28] J.B. Klauda, R.M. Venable, A.D. MacKerell Jr., R.W. Pastor, Considerations for lipid force field development, Curr. Top. Membr. 60 (2008) 1–48.
[29] M.A. Kastenholz, P.H. Hünenberger, Influence of artificial periodicity and ionic strength in molecular dynamics simulations of charged biomolecules employing lattice-sum methods, J. Phys. Chem. B 108 (2004) 774–788.
[30] M.M. Reif, V. Kräutler, M.A. Kastenholz, X. Daura, P.H. Hünenberger, Explicit-solvent molecular dynamics simulations of a reversibly-folding β-heptapeptide in methanol: influence of the treatment of long-range electrostatic interactions, J. Phys. Chem. B 113 (2009) 3112–3128.
[31] S. McLaughlin, The electrostatic properties of membranes, Annu. Rev. Biophys. Biophys. Chem. 18 (1989) 113–136.
[32] D.P. Tieleman, B. Hess, M.S.P. Sansom, Analysis and evaluation of channel models: simulation of alamethicin, Biophys. J. 83 (2002) 2393–2407.
[33] M. Patra, M. Karttunen, M.T. Hyvönen, E. Falck, P. Lindqvist, I. Vattulainen, Molecular dynamics simulations of lipid bilayers: major artifacts due to truncating electrostatic interactions, Biophys. J. 84 (2003) 3636–3645.
[34] M. Patra, M. Karttunen, M.T. Hyvönen, E. Falck, I. Vattulainen, Lipid bilayers driven to a wrong lane in molecular dynamics simulations by subtle changes in long-range electrostatic interactions, J. Phys. Chem. B 108 (2004) 4485–4494.
[35] A. Cordomí, O. Edholm, J. Perez, Effect of different treatments of long-range interactions and sampling conditions in molecular dynamic simulations of rhodopsin embedded in a dipalmitoyl phosphatidylcholine bilayer, J. Comput. Chem. 28 (2007) 1017–1030.
[36] Y. Takaoka, M. Pasenkievicz-Gierula, H. Miyagawa, K. Kitamura, Y. Tamura, A. Kusumi, Molecular dynamics generation of nonarbitrary membrane models reveals lipid orientational correlations, Biophys. J. 79 (2000) 3118–3138.
[37] A.H. de Vries, I. Chandrasekhar, W.F. van Gunsteren, P.H. Hünenberger, Molecular dynamics simulations of phospholipid bilayers: influence of artificial periodicity, system size, and simulation time, J. Phys. Chem. 109 (2005) 11643–11653.
[38] D.H. Herce, A.E. Garcia, Correction of apparent finite size effects in the area per lipid of lipid membranes simulations, J. Chem. Phys. 125 (2006), pp. 224711/1-224711/13.
[39] T. Baştuğ, S.M. Patra, S. Kuyucak, Finite system and periodicity effects in free energy simulations of membrane proteins, Chem. Phys. Lett. 425 (2006) 320–323.
[40] J.B. Klauda, B.R. Brooks, R.W. Pastor, Dynamical motions of lipids and a finite size effect in simulations of bilayers, J. Chem. Phys. 125 (2006) 144710/1–144710/8.
[41] D.P. Tieleman, S.J. Marrink, H.J.C. Berendsen, A computer perspective of membranes: molecular dynamics studies of lipid bilayers systems, Biochim. Biophys. Acta 1331 (1997) 235–270.
[42] S. Nagarajan, E.E. Schuler, K. Ma, J.T. Kindt, R.B. Dyer, Dynamics of the gel to fluid phase transformation in unilamellar DPPC vesicles, J. Phys. Chem. B 116 (2012) 13749–13756.
[43] N. Krog, K. Larsson, Phase behaviour and rheological properties of aqueous systems of industrial distilled monoglycerides, Chem. Phys. Lipids 2 (1968) 129–143.
[44] N. Krog, A.P. Borup, Swelling behaviour of lamellar phases of saturated monoglycerides in aqueous systems, J. Sci. Food Agr. 24 (1973) 691–701.
[45] I. Pezron, E. Pezron, B.A. Bergenstahl, P.M. Claesson, Repulsive pressure between monoglyceride bilayers in the lamellar and gel states, J. Phys. Chem. 94 (1990) 8255–8261.
[46] I. Pezron, E. Pezron, P.M. Claesson, B.A. Bergenstahl, Monoglyceride surface films: stability and interlayer interactions, J. Colloids Interface Sci. 144 (1991) 449–457.
[47] W.G. Morley, G.J.T. Tiddy, Phase behavior of monoglyceride/water systems, J. Chem. Soc. Faraday Trans. 89 (1993) 2823–2831.
[48] G. Cassin, C. de Costa, J.P.M. van Duynhoven, W.G.M. Agterof, Investigation of the gel to coagel phase transition in monoglyceride-water systems, Langmuir 14 (1998) 5757–5763.
[49] V. Chupin, J.-W.P. Boots, J.A. Killian, R.A. Demel, B. de Kruijff, Lipid organization and dynamics of the monostearoylglycerol-water system. A ^{2}H NMR study, Chem. Phys. Lipids 109 (2001) 15–28.
[50] A. Sein, J.A. Verheij, W.G.M. Agterof, Rheological characterization, crystallization, and gelation behavior of monoglyceride gels, J. Colloid Interface Sci. 249 (2002) 412–422.
[51] J.P.M. van Duynhoven, I. Broekmann, A. Sein, G.M.P. van Kempen, G.-J.W. Goudappel, W.S. Veeman, Microstructural investigation of monoglyceride-water coagel systems by NMR and CryoSEM, J. Colloid Interface Sci. 285 (2005) 703–710.
[52] C. Alberola, B. Blümich, D. Emeis, K.-P. Wittern, Phase transitions of monoglyceride emulsifier systems and pearlescent effects in cosmetic creams studied by ^{13}C NMR spectroscopy and DSC, Colloids Surf. A: Physicochem. Eng. Asp. 290 (2006) 247–255.
[53] D.R. Kodali, D.A. Fahey, D.M. Small, Structure and polymorphism of saturated monoacid 1, 2-diacyl-*sn*-glycerols, Biochemistry 29 (1990) 10771–10779.
[54] F.M. Goñi, A. Alonso, Structure and functional properties of diacylglycerols in membranes, Prog. Lip. Res. 38 (1999) 1–48.
[55] Y. Nishizuka, Protein kinase C and lipid signaling for sustained cellular responses, FASEB J. 9 (1995) 484–496.
[56] F. López-García, J. Villalaín, J.C. Gómez-Fernández, P.J. Quinn, The phase behavior of mixed aqueous dispersions of dipalmitoyl derivatives of phosphatidylcholine and diacylglycerol, Biophys. J. 66 (1994) 1991–2004.
[57] E. Berlin, E. Sainz, Acyl chain interactions and the modulation of phase changes in glycerolipids, Biochim. Biophys. Acta 855 (1986) 1–7.
[58] B.L. Li, S.M. Clarke, D.I. Wilson, Solid monolayers of glycerides adsorbed on the surface of graphite powder, Colloids Surf. A: Physicochem. Eng. Asp. 389 (2011) 180–187.
[59] N. Schmid, C.D. Christ, M. Christen, A.P. Eichenberger, W.F. van Gunsteren, Architecture, implementation and parallelisation of the GROMOS software for biomolecular simulation, Comput. Phys. Commun. 183 (2012) 890–903.
[60] A.-P.E. Kunz, J.R. Allison, D.P. Geerke, B.A.C. Horta, P.H. Hünenberger, S. Riniker, N. Schmid, W.F. van Gunsteren, New functionalities in the GROMOS biomolecular simulation software, J. Comput. Chem. 33 (2012) 340–353.
[61] W.F. van Gunsteren, The GROMOS Software for Biomolecular Simulation, 2015, Available from: http://www.gromos.net (accessed 05.05.11).
[62] B.A.C. Horta, P.F.J. Fuchs, W.F. van Gunsteren, P.H. Hünenberger, New interaction parameters for oxygen compounds in the GROMOS force field: improved pure-liquid and solvation properties for alcohols, ethers, aldehydes, ketones, carboxylic acids and esters, J. Chem. Theory Comput. 7 (2011) 1016–1031.
[63] H.J.C. Berendsen, J.P.M. Postma, W.F. van Gunsteren, J. Hermans, Interaction models for water in relation to protein hydration, in: B. Pullman (Ed.), Intermolecular Forces, Reidel, Dordrecht, The Netherlands, 1981, pp. 331–342.
[64] R.W. Hockney, The potential calculation and some applications, Methods Comput. Phys. 9 (1970) 135–211.
[65] J.-P. Ryckaert, G. Ciccotti, H.J.C. Berendsen, Numerical integration of the Cartesian equations of motion of a system with constraints: molecular dynamics of *n*-alkanes, J. Comput. Phys. 23 (1977) 327–341.
[66] S. Miyamoto, P.A. Kollman, SETTLE: an analytical version of the SHAKE and RATTLE algorithm for rigid water models, J. Comput. Chem. 13 (1992) 952–962.
[67] H.J.C. Berendsen, J.P.M. Postma, W.F. van Gunsteren, A. di Nola, J.R. Haak, Molecular dynamics with coupling to an external bath, J. Chem. Phys. 81 (1984) 3684–3690.
[68] W.F. van Gunsteren, S.R. Billeter, A.A. Eising, P.H. Hünenberger, P. Krüger, A.E. Mark, W.R.P. Scott, I.G. Tironi, Biomolecular simulation: The GROMOS96 Manual and User Guide, Verlag der Fachvereine, Zürich, Switzerland, 1996.
[69] W.F. van Gunsteren, H.J.C. Berendsen, Computer simulation of molecular dynamics: methodology, applications and perspectives in chemistry, Angew, Chem. Int. Ed. 29 (1990) 992–1023.
[70] J.A. Barker, R.O. Watts, Monte Carlo studies of the dielectric properties of water-like models, Mol. Phys. 26 (1973) 789–792.
[71] I.G. Tironi, R. Sperb, P.E. Smith, W.F. van Gunsteren, A generalized reaction field method for molecular dynamics simulations, J. Chem. Phys. 102 (1995) 5451–5459.
[72] T.N. Heinz, W.F. van Gunsteren, P.H. Hünenberger, Comparison of four methods to compute the dielectric permittivity of liquids from molecular dynamics simulations, J. Chem. Phys. 115 (2001) 1125–1136.
[73] Š. Perutková, M. Daniel, G. Dolinar, M. Rappolt, V. Kraj-Iglič, A. Iglič, Stability of the inverted hexagonal phas, in: A.L. Liu, H. Tien (Eds.), Advances in Planar Lipid Bilayers and Liposome, vol. 9., Elsevier, 2009, pp. 237–278.
[74] D.L. Dorset, W.A. Pangborn, Polymrphic forms of 1,2-dipalmitoyl-*sn*-glycerol: a combined X-ray and electron diffraction study, Chem. Phys. Lipids 48 (1988) 19–28.
[75] R.V. McDaniel, T.J. McIntosh, S.A. Simon, Nonelectrolyte substitution for water in phosphatidylcholine bilayers, Biochim. Biophys. Acta 731 (1983) 97–108.
[76] J.-P. Douliez, A. Ferrarini, E.-J. Dufourc, On the relationship between C-C and C-D order parameters and its use for studying the conformation of lipid acyl chains in biomembranes, J. Chem. Phys. 109 (1998) 2513–2518.

[77] W.L.C. Vaz, R.M. Clegg, D. Hallmann, Translational diffusion of lipids in liquid-crystalline phase phosphatidylcholine multibilayers - A comparison of experiment with theory, Biochemistry 24 (1985) 781–786.
[78] J.-P. Douliez, A. Léonard, E.J. Dufourc, Restatement of order parameters in biomembranes: calculation of C—C bond order parameters from C-D quadrupolar splittings, Biophys. J. 68 (1995) 1727–1739.
[79] J.-P. Douliez, A. Léonard, E.J. Dufourc, Conformational order of DMPC sn-1 versus sn-2 chains and membrane thickness: an approach to molecular protrusion by solid state ^{2}H NMR and neutron diffraction, J. Phys. Chem. 100 (1996) 18450–18457.
[80] J. Katsaras, D.S.C. Yang, R.M. Epand, Fatty-acid chain tilt angles and directions in dipalmitoyl phosphatidylcholine bilayers, Biophys. J. 63 (1992) 1170–1175.
[81] W.F.D. Bennett, J.L. MacCallum, M.J. Hinner, S.J. Marrink, D.P. Tieleman, Molecular view of cholesterol flip-flop and chemical potential in different membrane environments, J. Am. Chem. Soc. 131 (2009) 12714–12720.
[82] R. Chen, D. Poger, A.E. Mark, Effect of high pressure on fully hydrated DPPC and POPC bilayers, J. Phys. Chem. B 115 (2011) 1038–1044.